Pergamon

Atmospheric Environment Vol. 32, No. 18, pp. 3105–3112, 1998

Printed in Great Britain

PII: S1352–2310(97)00503–7

1352–2310/98 $19.00 + 0.00

TURBULENT DISPERSION OF AIRCRAFT EXHAUSTS IN REGIONS OF BREAKING GRAVITY WAVES

ANDREAS DÖRNBRACK and TILMAN DÜRBECK*

DLR Oberpfaffenhofen, Institut für Physik der Atmosphäre, D-82230 Weßling, Germany

(*First received* 13 *May* 1997 *and in final form* 15 *November* 1997. *Published July* 1998)

Abstract—This study describes the three-dimensional dispersion of aircraft exhausts released into regions of overturning and breaking gravity waves below a critical level. The principal concept is to estimate effective diffusivities of a passive scalar by combining previous numerical approaches to the plume dispersion in the free atmosphere and to the breakdown of internal gravity waves at those altitudes. Here, it could be shown that the possible high vertical diffusivity of $6\,m^2\,s^{-1}$ contributes considerably to an efficient vertical mixing of aircraft exhausts or other species, e.g. trace gases. The effective vertical diffusion coefficient of the entire breaking event is calculated to be $D_v^{eff} \approx 0.5\,m^2\,s^{-1}$. © 1998 Elsevier Science Ltd. All rights reserved

1. MOTIVATION

Since recently, there has been increased awareness of the effects of high flying aircraft on the state of the atmosphere of our planet and much publicity has been drawn to the long-term effects of emitted exhaust gases (Schumann, 1995, 1997; Stolarski, 1995). To determine the impact of an aircraft exhaust gas onto the atmosphere it is crucial to understand how that pollutant mixes with the ambient air. The whole spectrum of atmospheric motions is important here—even the dilution processes on small scales. However, the identification of mixing mechanisms in the stably stratified free atmosphere continues to be a difficult task. One mechanism contributing to the generation of turbulence results from the amplification of a Kelvin–Helmholtz instability which arises in regions of strong shear surrounded by regions of low shear (cf. recent simulations of Scinocca, 1996; Fritts *et al*., 1997). Moreover, breaking internal gravity waves have been thought to form relatively thin turbulent layers in the free atmosphere (Vinnichenko *et al*., 1976). Internal gravity waves break due to increasing amplitudes (caused by an exponential density decrease with height) or due to local convective and dynamical instabilities (resulting from an interaction of the wave with a critical level). At a critical level, the phase speed of the wave equals the horizontal velocity of the mean flow (cf. e.g. Baines, 1995, Chap. 4.11 for an introductory text). This mechanism has been intensively investigated by Winters and d'Asaro (1994), Fritts *et al*. (1996) and Dörnbrack (1997) during the last couple of years.

Atmospheric observations of all these small-scale mixing processes are very rare and restricted to some singular case studies (e.g. Kennedy and Shapiro, 1980; Bedard *et al*., 1986; Nastrom and Eaton, 1993; Worthington and Thomas, 1996). Most of previous observational efforts to determine effective mixing parameters in the free atmosphere are motivated by the phenomenon of clear-air turbulence (Pao and Goldburg, 1969; Crane, 1980; Tank, 1994). The general strategy was to identify (and later to forecast) regions of enhanced vertical diffusivity D_v^{eff} or, equivalently, of high-energy dissipation rates ε. Lilly *et al*. (1974) analysing the HICAT data estimated $D_v^{eff} \approx 0.25\,m\,s^{-2}$ from power spectra of velocity fluctuations assuming $D_v^{eff} \propto \varepsilon/N^2$, where N is the Brunt–Väisälä frequency. The radar measurements of Woodman and Rastogi (1984) give the same value, whereas Sato and Woodman (1982) distinguish between tropospheric ($D_v^{eff} \approx 0.3\,m\,s^{-2}$) and stratospheric ($D_v^{eff} \approx 0.1\,m\,s^{-2}$) transport properties. The balloon measurements of Cadet (1975, 1977) and Barat (1982, 1983) lead to values of D_v^{eff} between 0.01 and $0.1\,m\,s^{-2}$, based again on power spectra. Recent balloon observations with a vertical resolution of 20 cm revealed the existence of vertically separated layers of strong thermal stability (thickness of up to 20 m with vertical temperature gradients of up to 10 K/100 m) and layers dominated by turbulent mixing (Dalaudier *et al*., 1994). The mixed layers are about 1–100 m thick

*Current affiliation: Siemens AG, Hofmannstr. 51, D-81359 München, Germany. E-mail: pa2o@atlas.op.dr.de

and their occurence is well correlated with the existence of vertically propagating gravity waves.

Other estimates of D_v^{eff} are based on numerical simulations of mixing processes in the free atmosphere. Schilling and Etling (1996) studied the two-dimensional dispersion of aircraft plumes in breaking gravity waves. A Lagrangian particle model allowed to estimate an effective diffusion coefficient for the entire breaking event of about $0.7\,m\,s^{-2}$. Dürbeck and Gerz (1995, 1996) investigated homogeneous atmospheric conditions with and without shear where the turbulence decays with time. The length scale of the turbulent eddies was of the order of the exhaust plume diameter. In these three-dimensional large-eddy simulations, typical mean characteristics of the predominantely quiet free atmosphere were prescribed in terms of the mean vertical wind shear S and the Brunt–Väisälä frequency N, leading to bulk Richardson numbers ranging from 0.1 to ∞. The dispersion of a large ensemble of aircraft plumes was analysed statistically. For Richardson numbers larger than 1, the effective vertical diffusivity D_v^{eff} did not exceed values of $0.18\,m\,s^{-2}$. The shearless case constituted the lower limit for D_v^{eff} of $0.15 \pm 0.01\,m\,s^{-2}$. Only for the low Richardson number of 0.13 the simulations lead to values for D_v^{eff} as high as about $3\,m\,s^{-2}$.

Along flight legs of commercial aircrafts the ambient air is usually weakly turbulent and turbulence encounters occur only occasionally. This exceptional case is considered here. It is supposed that rare but intense turbulent events contribute to an effective vertical mixing at least as much as the diffusion under decaying turbulent conditions. For this purpose, this study is concerned with the dispersion of exhaust plumes released at cruising altitudes into regions of localised generated turbulence. Here, the breaking of internal gravity waves below a critical level is simulated by the same high-resolution numerical model as presented by Dörnbrack (1997) and completed by the integration of passive scalars. The parameters of the background flow conditions and of the aircraft plumes are taken from Dürbeck and Gerz (1996). The dominant vertical and horizontal scales of this problem are of the order of about 100 m to 1 km. These scales are larger than the diameter of wake vortices directly behind the aircraft (50 m) and much smaller than meteorological disturbances of mesoscale extent ($\approx 200 \ldots 500$ km).

2. SET-UP OF THE NUMERICAL EXPERIMENTS

The numerical experiments described here are three-dimensional, high-resolution simulations of the dispersion of two-dimensional aircraft plumes released into a region of breaking gravity waves. The three-dimensional breaking of internal gravity waves beneath a critical level is simulated by the same model as described by Dörnbrack (1997) (cf. Fig. 1): a uniform shear flow over a wavy wall generates vertically propagating gravity waves in a stably stratified Boussinesq fluid. These waves turn over and become unstable beneath the critical level where a turbulent mixed layer evolves.

The flow is simulated in a rectangular box with coordinates x, y, and z, where y is the flight direction of the airplanes and z the vertical direction. The side lengths of the box are the same as in the study of Dürbeck and Gerz (1996), i.e. $L_x = 4L_y = 4H$, where $H = 1068$ m. The initial velocity and temperature fields are given by

$$U(z) = \bar{S}(z - 0.5H), \quad \text{where } \bar{S} = \frac{\Delta U}{H}$$

and

$$\Theta(z) = \vartheta_0 + \frac{\Delta\Theta}{H}(z - 0.5H), \quad \text{where } \frac{\Delta\Theta}{H} = \frac{N^2\vartheta_0}{g} \qquad (1)$$

where the Brunt–Väisälä frequency is $N = 0.006\,s^{-1}$ and the velocity difference between top and bottom amounts to $\Delta U = 5.5\,m\,s^{-1}$. These values are taken from case No. 5 of Dürbeck's and Gerz's study (1996).

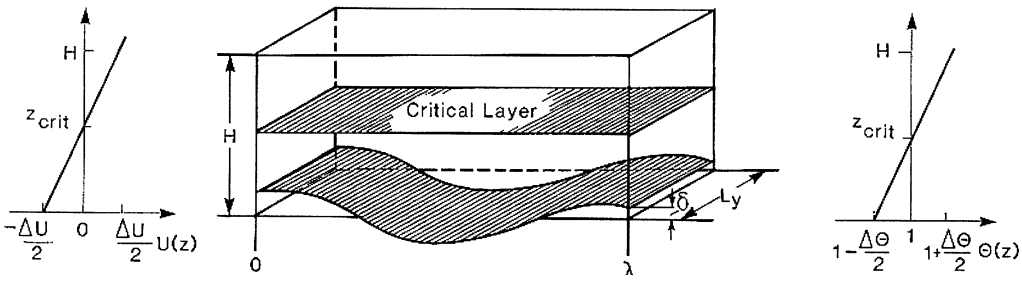

Fig. 1. Schematic sketch of the computational domain and the background flow conditions. The amplitude of the surface wave is $\delta = 0.04H$, its wavelength is $\lambda = 4H$, where $H = 1068$ m is the vertical depth of the domain. The length of the cross stream direction (identical to the flight direction) is $L_y = H$. The critical layer z_{crit} is defined by $U = 0$. The velocity and temperature differences ΔU and $\Delta\Theta$ across H are chosen in such a way that the bulk Richardson number $Ri_B = (g/\vartheta_o)\Delta\Theta/H/(\Delta U/H)^2$ is approximately 1.4 at the beginning.

The bulk Richardson number $Ri_B = N^2/\bar{S}^2$ is approximately 1.4 at the beginning of the simulation.

Dürbeck and Gerz (1995, 1996) considered the effective diffusion of aircraft emissions in the stably stratified free atmosphere under shearless and sheared conditions. There, homogeneous turbulence is initialized in the whole domain by random fields of anisotropic velocity components with prescribed spectra. The turbulence decays and ceases when time progresses as long as the mean wind shear is not very strong. The situation described in the present paper is different: the turbulence is generated locally by convective and dynamical instabilities caused by overturning gravity waves. Therefore, the initial flow field is slightly disturbed by small random temperature perturbations, otherwise, the flow would remain two dimensional for all times.

The amplitude of the surface wave is $\delta = 0.04H$, its length $\lambda = 4H$. The short wavelength limit for internal gravity waves is given by $2\pi U/N$, where U is the horizontal wind speed. Hence, for given N and λ, the atmospheric wind speed is restricted to values below $5\,\mathrm{m\,s^{-1}}$. Otherwise, no internal gravity waves would exist. Further details of the numerics and boundary conditions of the dynamical model can be found in Dörnbrack *et al.* (1995) and Dörnbrack (1997).

Three plumes ($\alpha = 1, 2, 3$) with a Gaussian concentration distribution on the xz-plane and equally distributed in the flight direction y

$$c^{\alpha}(x, z, t_{\mathrm{rel}}) = \frac{1}{2\pi\sigma_{\mathrm{ho}}\sigma_{\mathrm{vo}}L_y}\exp\left\{-\frac{1}{2}\left(\frac{(x-x_c^{\alpha})^2}{\sigma_{\mathrm{h,o}}^2}+\frac{(z-z_c)^2}{\sigma_{\mathrm{v,o}}^2}\right)\right\} \quad (2)$$

are released at different horizontal locations $x_c^{\alpha} = 0.4$, 0.6, and 0.8λ and below the critical level at $z_c = 0.35H$. In addition to studying the supposed dependence of the dispersion on the initial plume location, their temporal evolution is investigated for five successive release times $t_{\mathrm{rel}} = 16, 22, 28, 32,$ and $36\,t_{\mathrm{ref}}$, where $t_{\mathrm{ref}} = H/\Delta U = 194\,\mathrm{s} \approx 3\,\mathrm{min}$. Altogether, the dispersion of 15 exhaust plumes is simulated. The maximum integration time is $60\,t_{\mathrm{ref}}$, i.e. about 3 h. All numerical experiments are carried out using grids with $256 \times 64 \times 96$ points in the x, y, and z directions, i.e. the spatial resolution is (16.7, 16.7, 11.3 m).

The quantities $\sigma_{\mathrm{h,o}}^2$ and $\sigma_{\mathrm{v,o}}^2$ in equation (2) are the horizontal (in x-direction) and the vertical variances of the concentration distribution at t_{rel}. The present simulations of the plume dispersion starts at the end of the so-called dispersion regime (CIAP, 1975). At this stage of plume evolution, the aircraft induced turbulence is ceased (Schumann *et al.*, 1995). By then, the exhaust gases are mixed over a finite volume with the ambient air and the exhaust plumes can be represented by a line source according to equation (2) where the initial values $\sigma_{\mathrm{h,o}} = 117\,\mathrm{m}$ and $\sigma_{\mathrm{v,o}} = 83\,\mathrm{m}$ are taken from observations of 10 min old contrails by Schumann *et al.* (1995).

3. RESULTS

3.1. *Flow structure*

Before the dispersion of exhaust plumes will be discussed, a brief overview of the simulated flow evolution is given. According to Dörnbrack (1997), the gravity-wave breaking process can be divided into three principal periods. During the first period, stationary gravity waves with respect to topography are induced by the flow over the fixed wavy surface. Above the critical level, no or very small, damped wavy disturbances are observed. Below the critical level, the main effect is the long lasting acceleration of the mean flow in the positive x-direction. This wave-induced acceleration due to the deposit of horizontal momentum is opposite to the direction of $U(z)$. The disturbed mean flow raises heavier fluid over lighter one directly beneath the critical level, whereas the mean advection in the negative x-direction at lower altitudes moves lighter fluid under heavier one. Between these levels, the fluid stagnates and a convectively unstable region extending over almost one wavelength λ and with a thickness of about 100 m is formed. The left column of Fig. 2 displays the evolving temperature field from the end of the first period (a) towards the second period, where an eruptive convective instability leads to a first turbulent breakdown after about 100 min simulation time (Figs 2c and d). It takes about six Brunt–Väisälä periods ($T_{\mathrm{BV}} = 2\pi/N \approx 17.5\,\mathrm{min}$) until the instability grows to three-dimensional motions. The developing mixed layer (cf. left column of Fig. 3) is organized in shear-driven overturning rolls with axes in cross-stream direction and in counterrotating streamwise vortices (not displayed here, cf. Dörnbrack, 1997). The streamwise vortices derive their energy mainly from buoyancy, later shear dominates. The flow in the mixed layer is random and vertical on a wide range of scales. The dominant horizontal scale in the range of 800–1200 m is larger than the vertical scale of maximum 250 m. The third and last stage of flow evolution is characterized by a quasi-steady equilibrium between shear production and mechanical dissipation of turbulent kinetic energy. The final thin mixed layer consists of isolated patches of turbulence embedded in a smooth mean flow that lead to the sporadic occurrence of turbulent events at fixed locations.

3.2. *Plume dispersion*

The first three sets of the plumes (left = black, middle = blue, and right = red) are emitted during the first period of flow evolution (at 52, 71, and 90 min), the other two during the second period (at 104 and 116 min). Exemplary for the first group, the right column of Fig. 2 displays the plume dispersion of the second set whereas the sequence of concentration fields in Fig. 3 depicts the development for the last set. Both figures cover the same interval of $12\,t_{\mathrm{ref}} \approx 40\,\mathrm{min}$.

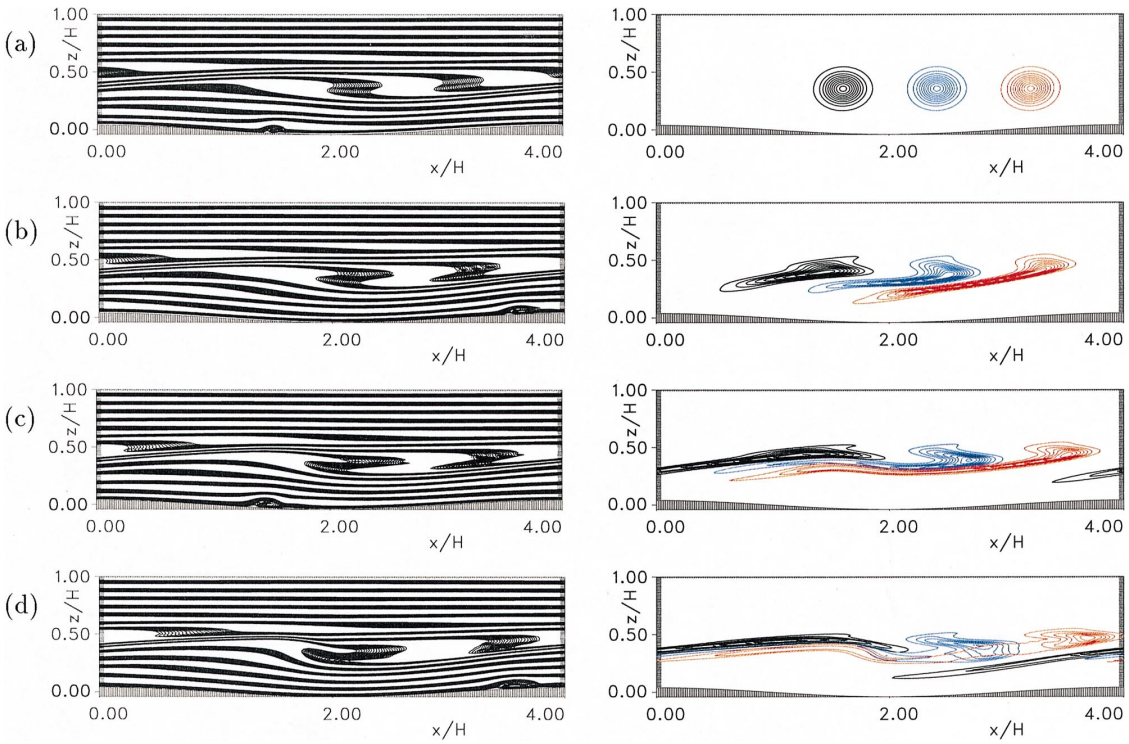

Fig. 2. Contours plots of the y-averaged temperature (left) and concentration fields (right) evolving in time. The three Gaussian plumes (cf. equation (2)) are emitted instantaneously at $t = 71$ min (a) after model initialization. The temporal interval between the panel rows (a) to (d) is 13 min. The thickness of the black temperature segments amounts to $0.007\Delta\Theta$. Broader (thinner) segments indicates reduced (enhanced) thermal stability. The contour levels of the concentration field are equidistant and are chosen uniformly for all plots.

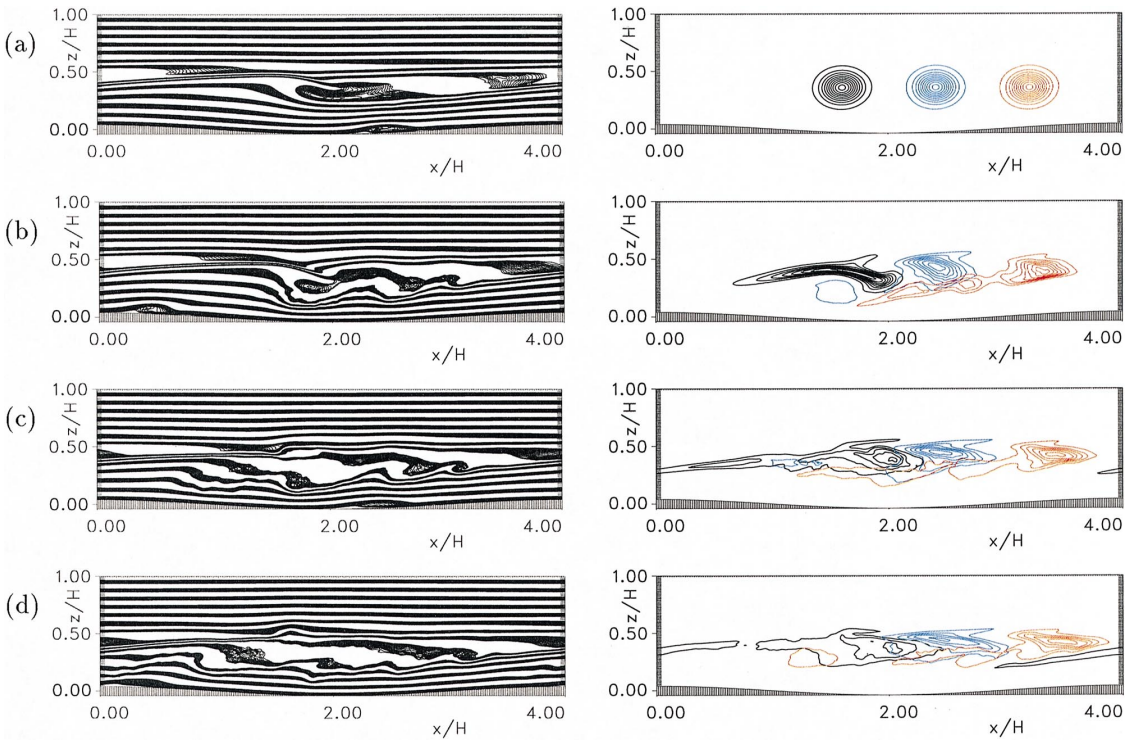

Fig. 3. As Fig. 2 for a plume released at $t = 116$ min after model initialization. Again, the temporal interval between the panel rows is 13 min.

The most remarkable feature of the sequence shown in Fig. 2 is the rapid horizontal spread of the lower portions of all three plumes into the downstream direction while their upper portions remain almost stationary. The weak deformation and advection of the upper parts is a product of the nearly zero horizontal velocity close to the critical level. However, there is a horizontal drift of the red (black) plume towards right (left) due to the wave-induced acceleration of the mean flow. This additional advection fully affects the uppermost portion of the red plume and only the lower portions of the blue and black ones. The resulting advection which is modified by waves and dependent on height forms the characteristic S-shape of both plumes (Figs 2b and c). The lower portions of the concentration distributions are controlled by shear deformation and their structures remind of findings by Dürbeck and Gerz (1996) where the prescribed uniform shear causes a symmetrical stretching of isocontours with respect to the centre of mass. In the present study, the horizontal spread depends strongly on the local wind field, i.e. on the individual location of plume release. The vertical spread depends on the horizontal release position, too. In this stage of flow evolution, the vertical spread is not yet affected by three-dimensional turbulent motions. The vertical expansion is mainly produced by wave-induced vertical motions (upwards/downwards for flows in the luv/lee of the crest) that transport exhaust gases into layers of different horizontal velocity. The height-vs-time plots of the locations of maximum concentration confirm that the outer plumes undergo the most vigorous vertical excursions (Fig. 4a) : the red (black) plume is finally displaced upwards (downwards) whereas the slowly dispersing blue plume remains essentially at the same height.

The dispersion of aircraft exhausts emitted at $t = 116$ min (which is six minutes later than the time at which the fields are shown in Fig. 2) reveals the dominant influence of the beginning turbulent diffusion, esp. that of the black plume (cf. Fig. 3). Initially, its dispersion evolves similarly as in the previous example. In addition, there occurs a horizontal spread towards the positive x-direction due to the overturning wave in this region. It is the turbulent breakdown of this wave that mixes and dilutes this plume very quickly (Figs 3c and d). Likewise, separated portions of the other plumes that are advected into the breaking region get diffused more intense than their almost stationary parts. Later, smaller scale, shear induced rolls dilute these remaining coherent plume regions with ambient air. At the end, the concentration distributions of all plumes are much more diluted compared to plumes emitted at earlier times. Obviously, the spread of the plumes dominated by advection is substituted by turbulent mixing in the breaking region at this stage. The height-vs-time plot in Fig. 4b exhibits the same vertical thickness of the layer and altitude of plume maxima at late times. This vertical uniformity is generated by the violent vertical mixing

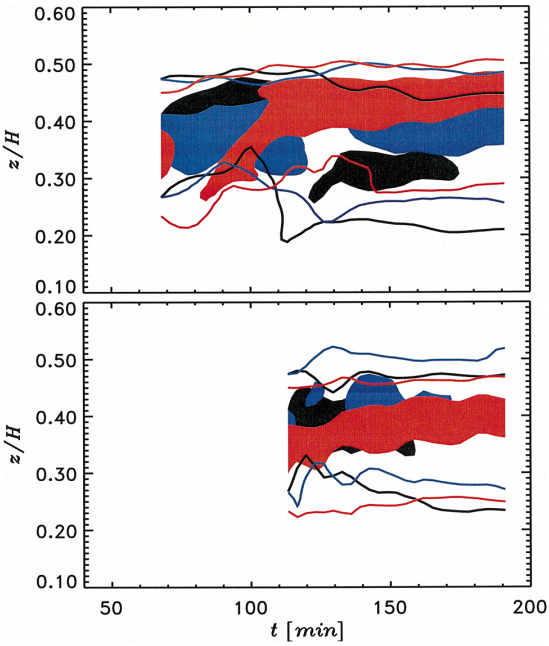

Fig. 4. Height-time plots for the horizontally averaged concentration fields of the plume evolution shown in Figs 2 (top) and 3 (bottom). The coloured regions mark layers where the dimensionless concentration is greater than 1.1, the solid lines are for $c = 0.5$. The colours refer to the three plumes released at different horizontal positions.

and the absence of wave-like motion in the turbulent region. In summary, the structure of the concentration distribution of the dispersing exhaust gases depends strongly on the time and location of plume release relative to the state of the turbulence production by the breaking gravity waves.

3.3. *Diffusivities*

In order to quantify the mixing properties, this section presents the time series of the coordinates of the centre of mass (x_s, z_s) (shown in Fig. 5) as well as those of the horizontal and vertical variances σ_h^2 and σ_v^2 (shown in Fig. 6) of each plume. The statistics are based on the data of the y-averaged, two-dimensional concentration fields.

The influence of advective effects on the locations of centre of the gravity (x_s, z_s) is revealed by their horizontal and vertical displacements displayed in Fig. 5. Shortly after their emission, all outer plumes are moved vertically according to the local vertical velocity field (the black plume upwards, the red plume downwards). Due to the simultaneous horizontal drift, the plumes enter regions of different vertical velocity or zones where turbulent mixing initiates strong vertical displacements. Altogether, the centres of mass of the red plumes are raised and shifted upstream, whereas those of the black plumes descend after a long downstream advection. As expected, the blue plumes are only slightly affected by advective processes. The horizontal excursions are the smaller

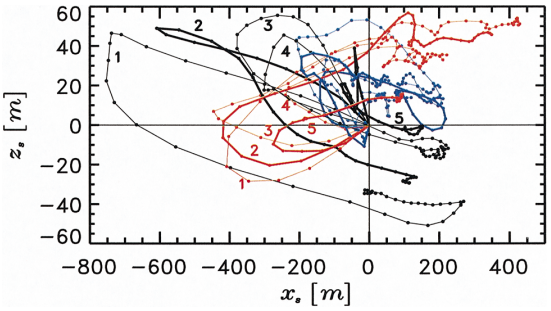

Fig. 5. Temporal evolution of the location of centre of mass (x_s, z_s) for all plumes. The colours refer to the initial plume positions and the numbers denote the temporal order of emission. The dots separate one dimensionless time unit $t_{ref} \approx 3$ min. The thick lines are for the plumes depicted in Figs 2 and 3.

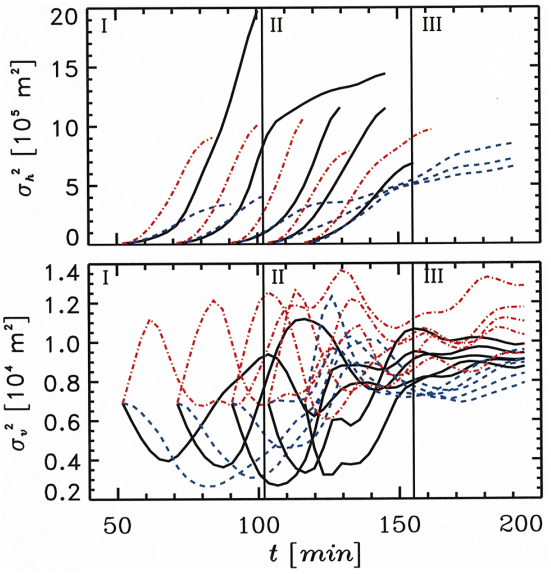

Fig. 6. Temporal evolution of the horizontal (top) and vertical variances (bottom) for all plumes. The colours refer to the three plumes released at different horizontal positions. The segments I to III separate the three principal periods of flow evolution (I – two dimensional wave propagation, II – overturning and breakdown of the gravity wave, III – quasi-steady mixed layer).

the later plumes are emitted because the advective effects are gradually becoming less important and are superimposed by turbulent diffusion.

The horizontal variances σ_h^2 of the concentration fields of all plumes grow with higher rates than those of plumes released under the same background flow conditions but without disturbances due to propagating and breaking gravity waves (cf. Fig. 6). For the latter situation Dürbeck (1997) found that σ_h^2 grows within 1 h of diffusion time to values of about 1×10^5 m^2. In the present study we found values up to 2×10^6 m^2. It must be noted that the evaluation of σ_h^2 was stopped when the extension of the plumes started to exceed that of the horizontal domain size and the results for σ_h^2 are therefore corrupted. The quickest horizontal growth is that of the red plumes because they are introduced into a region of high shear leading to large horizontal spread. The blue and black plumes expand horizontally at the same rate for early diffusion times. Later, the blue plumes grow much slower than the black ones due to dominating turbulence in the middle of the domain. The turbulent mixing is also responsible for the smaller slope of σ_h^2 for both blue plumes released in the second period of flow evolution.

The evolution of the vertical variances σ_v^2 with time differs significantly from that one of the cases documented by Dürbeck (1997). Generally, in the first 30 min after release the red plumes become vertically thicker whereas the other plumes become thinner with time. This is a result of locally strong shear and the inhibiting effect of the critical level for vertical upwards motions that confines the plume below the critical level. Finally, this leads to the strong plume stretching beneath the critical level and to decreasing σ_v^2. The exhaust gases are transported downwards (upwards) for locations right (left) of the surface trough. The downward motion of the red plumes also causes their rapid horizontal dispersion as the exhaust gases are transported into regions of higher horizontal velocity. In the second period of the flow evolution the vertical variances grow due to the beginning turbulent diffusion up to $\sigma_v^2 \approx 1.4 \times 10^4$ m^2. At the end of the simulations and for all plumes, σ_v^2 is greater than the initial value $\sigma_{v,o}^2$. Interestingly, the final values cover the same range of $\sigma_v^2 \approx 0.8 \ldots 1.3 \times 10^4$ m^2 as those given by Dürbeck (1997) whereby the largest values are obtained for the red, the lowest values for the blue plumes.

Dürbeck and Gerz (1996) calculated effective dispersion coefficients under sheared conditions assuming that the shape of the expanded plumes approximately remained Gaussian. Due to the varying deformation of the plumes under the influence of propagating and breaking gravity waves this refined technique cannot be applied here. Therefore, and as a first approximation, the effective dispersion coefficients are calculated by $D_{h,v}^{eff} = 0.5\, d\sigma_{h,v}^2/dt$ for the second and last period of flow evolution when advection influences the plume dispersion only marginally.

The horizontal dispersion coefficient for both outer plumes reaches temporarily values up to 600 m s^{-2}. However, this value is solely produced by continuing advective processes that elongate the plumes as discussed before. It is the blue plume only that can be used for estimating the turbulent diffusion. Its horizontal diffusivity never exceeds 150 m^2 s^{-1} whereby an arithmetic mean in the second and third period yields $D_h^{eff} = 60 \pm 5$ m^2 s^{-1}. The effective vertical dispersion coefficients are generally smaller. In the turbulent period, D_v^{eff} is maximum 6 m^2 s^{-1}, at the end values of 2 m^2 s^{-1} are not exceeded.

Numerical models of large-scale atmospheric dynamics require spatially and temporally averaged values of coefficients of turbulent viscosity. Therefore, it is noteworthy to evaluate an effective vertical dispersion coefficient for the whole wave breaking event. This quantity is estimated as the ratio of the total increase of σ_v^2 to the respective time period:

$$\bar{D}_v^{\text{eff}} = \frac{1}{\text{np}} \sum_{\text{np}} \frac{1}{2} \frac{\sigma_v^2(t_{\text{end}}) - \sigma_{v,o}^2}{t_{\text{end}} - t_{\text{rel}}} \approx 0.5\,\text{m}^2\,\text{s}^{-1}$$

where np is the number of all plumes. Effective dispersion coefficients as above can be used to parameterise the subgrid-scale diffusion of passive scalars in larger scale numerical models.

4. DISCUSSION AND CONCLUSIONS

This study is concerned with the determination of effective diffusivities of aircraft emissions in regions of intermittent and patchy turbulence at cruising altitudes. For this purpose, the dispersion of various plumes is investigated by means of high-resolution numerical simulations. Fully developed turbulence is very rare at flight altitudes and exhaust gases are emitted only occasionally in these regions. However, for these circumstances, it has been shown that turbulent mixing on short time and space scales can dilute passive tracers very efficiently. This study is not solely restricted to the dispersion of aircraft exhausts and the results are applicable for other species as, e.g. trace gases, too.

During the breaking event maximum effective vertical diffusivities of $6\,\text{m}^2\,\text{s}^{-1}$ are reached. The temporal evolution of the plume dispersion depends strongly on the time and location of plume release relative to the state of the breaking gravity wave. Two effects produce the horizontal spread of the plumes: the advection which is modified by gravity waves and dependent on height and the spontaneously starting turbulent diffusion inside the convectively unstable layer of the overturning wave. The mean vertical diffusivity of the whole breaking event is estimated to be $\bar{D}_v^{\text{eff}} \approx 0.5\,\text{m}^2\,\text{s}^{-1}$. Strikingly, this value is about 3 times larger than that evaluated by Dürbeck and Gerz (1996) for the same background flow conditions but without wave breaking. Moreover, the same range of values of the vertical variance σ_v^2 after about one hour of diffusion time shows that the short period and localised wave breaking event contributes to the vertical diffusion at least as much as the decaying homogeneous turbulence investigated by Dürbeck and Gerz (1996). Generally, the magnitude of the estimated effective vertical diffusivity agrees well with former observations and calculations mentioned in Section 1.

The main goal of the present and previous studies has been to estimate the effective diffusivities. This is an essential input for forecasting the effects of high-flying aircrafts on the future state of the global atmosphere. Turbulent diffusivities of our studies have already been used in box models describing the evolution of the exhaust composition in and out the atlantic flight corridor (see e.g. Karol *et al*., 1997). Further applications to large-scale atmospheric models require a balanced approach between the artificial numerical diffusion in these models and the physically determined diffusivities.

Acknowledgements—This work was supported by the Deutsche Forschungsgemeinschaft (DFG) in the framework of the Schwerpunktprogramm "Grundlagen der Auswirkungen der Luft- und Raumfahrt auf die Atmosphäre".

REFERENCES

Baines, P. G. (1995) *Topographic Effects in Stratified Flows*. 482 pp. Cambridge University Press, Cambridge.

Barat, J. (1982) Some characteristics of clear-air turbulence in the middle stratosphere. *Journal of Atmospheric Sciences* **39**, 2553–2564.

Barat, J. (1983) The fine structure of the stratospheric flow revealed by differential sounding. *Journal of Geophysical Research* **88**, 5219–5228.

Bedard, A. J., Canavero, F. and Einaudi, F. (1986) Atmospheric gravity waves and aircraft turbulence encounters. *Journal of Atmospheric Science* **43**, 2838–2844.

Cadet, D. (1975) Vertical wind shear measurements in the lower stratosphere. *Quarterly Journal of Royal Meteorological Society* **101**, 485–493.

Cadet, D. (1977) Energy dissipation within intermittent clear air turbulence. *Journal of Atmospheric Sciences* **34**, 137–142.

CIAP (1975) *Final Report*, *Department of Transportation*, *Climatic Impact Assessment Program*, Vol. 2, Ch. 2, DOT-TST-75-53.

Crane, R. K. (1980) A review of radar observations of turbulence in the lower stratosphere. *Radio Science* **15**, 177–193.

Dalaudier, F., Sidi, C., Crochet, M. and Vernin, J. (1994) Direct evidence of "sheets" in the atmospheric temperature field. *Journal of Atmospheric Sciences* **51**, 237–248.

Dörnbrack, A. (1997) Turbulent mixing by breaking gravity waves. *Journal of Fluid Mechanics* submitted.

Dörnbrack, A., Gerz, T. and Schumann, U. (1995) Turbulent breaking of overturning gravity waves below a critical level. *Applied Scientific Research* **54**, 163–176.

Dürbeck, T. (1997) *Grobstruktursimulation von Mischungsprozessen in der freien Atmosphäre*. DLR-Forschungsbericht 97-02, 96 pp.

Dürbeck, T. and Gerz, T. (1995) Large-eddy simulation of aircraft exhaust plumes in the free atmosphere: effective diffusivities and cross-sections. *Geophysical Research Letters* **22**, 3203–3206.

Dürbeck, T. and Gerz, T. (1996) Dispersion of aircraft exhausts in the free atmosphere. *Journal of Geophysical Research* **101**, 26007–26015.

Fritts, D. C., Isler, J. R. and Andreassen, Ø. (1994) Gravity breaking in two and three dimensions. 2. Three-dimensional evolution and instability structure. *Journal of Geophysical Research* **99**, 8109–8123.

Fritts, D. C., Garten, J. F. and Andreassen, Ø. (1997) Wave breaking and transition to turbulence in stratified shear flows. *Journal of Atmospheric Sciences* **53**, 1057–1085.

Karol, I. I., Ozolin, Y. E. and Rozanov, E. V. (1997) Box and gaussian plume models of the exhaust composition evolution of subsonic transport aircraft in and out of the flight corridor. *Annales de Geophysicae* **15**, 88–96.

Kennedy, P. J. and Shapiro, M. A. (1980) Further encounters with clear air turbulence in research aircraft. *Journal of Atmospheric Sciences* **37**, 986–993.

Lilly, D. K., Waco, D. E. and Adelfang, S. I. (1974) Stratospheric mixing estimated from high-altitude turbulence measurements. *Journal of Applied Meteorology* **13**, 488–493.

Nastrom, G. D. and Eaton, F. D. (1993) The coupling of gravity waves and turbulence at White Sands, New Mexico, from VHF radar observations. *Journal of Applied Meteorology* **32**, 81–87.

Pao, Y. and Goldburg, A. (eds.) (1969) *Clear Air Turbulence and its Detection*. Plenum Press, New York.

Sato, K. and Woodman, R. F. (1982) Fine altitude resolution radar observations of stratospheric layers by the Arecibo 430 MHz radar. *Journal of Atmospheric Sciences* **39**, 2546–2552.

Schilling, V. and Etling, D. (1996) Vertical mixing of passive scalars owing to breaking gravity waves. *Dynamic Atmospheric Oceans* **23**, 371–378.

Schumann, U. (Ed.) (1995) *AERONOX – The impact of* NO_X *emissions from aircraft upon the atmosphere at flight altitudes* 8–15 *km* Publication EUR 16209 EN, ISBN-92-826-8281-1, Office for Publications of the European Commission, Brussels, 471 pp.

Schumann, U. (Ed.) (1997) *Pollution from aircraft emissions in the North Atlantic flight corridor* (*POLINAT*) . Final report to the Commission of the European Communities, EV5V-CT93-0310 (DG12 DTEE), EUR 16987.

Schumann, U., Konopka, P., Baumann, R., Busen, R., Gerz, T., Schlager, H., Schulte, P. and Volkert, H. (1995) Estimate of diffusion parameters of aircraft exhaust plumes near the tropopause from nitric oxide and turbulence measurements. *Journal of Geophysical Research* **100**, 14,147–14,162.

Scinocca, J. F. (1996) The mixing of mass and momentum by Kelvin-Helmholtz billows. *Journal of Atmospheric Sciences* **52**, 2509–2530.

Stolarski, R. S. (Ed.) (1995) 1995 *Scientific assessment of the atmospheric effects of stratospheric aircraft*. NASA Reference Publication 1381, NASA, Washington, D.C., 95 pp.

Tank, W. (1994) *A climatology of lower stratosphere clear air turbulence*. AIAA 94–0377.

Vinnichenko, K. N., Pinus, N. Z., Shmeter, S. M. and Shur, G. N. (1976) *Turbulence in the free atmosphere*, Hydrometeoizdat, Leningrad, 287 pp.

Winters, K. B. and D'Asaro, E. A. (1994) Three-dimensional wave instability near a critical level. *Journal of Fluid Mechanics* **272**, 255–284.

Woodman, R. F. and Rastogi, P. K. (1984) Evaluation of effective eddy diffusive coefficients using radar observations of turbulence in the stratosphere. *Geophysical Research Letters* **11**, 243–246.

Worthington, R. M. and Thomas, L. (1996) Radar measurements of critical layer absorption in mountain waves. *Quarterly Journal of Royal Meteorological Society* **122**, 1263–1282.